Available online at www.sciencedirect.com
SCIENCE DIRECT®
Journal of Nuclear Materials 320 (2003) 106–116
journal of nuclear materials
www.elsevier.com/locate/jnucmat

The EFTTRA-T3 irradiation experiment on inert matrix fuels

E.A.C. Neeft [a], K. Bakker [a], R.P.C. Schram [a,*], R. Conrad [b], R.J.M. Konings [c]

[a] Nuclear Research Consulting Group (NRG), P.O. Box 25, 1755 ZG Petten, The Netherlands
[b] European Commission, Joint Research Centre, Institute for Energy, P.O. Box 2, 1755 ZG Petten, The Netherlands
[c] European Commission, Joint Research Centre, Institute for Transuranium Elements, Postfach 2340, 76125 Karlsruhe, Germany

Abstract

In the EFTTRA-T3 irradiation experiment eight uranium bearing inert matrix fuel capsules and eight capsules containing inert matrices have been irradiated. The irradiations were based on the matrices: MgO, $MgAl_2O_4$, $Y_3Al_5O_{12}$, Y_2O_3 and CeO_2. The heterogeneously dispersed fuel contained fissile inclusions of UO_2 or $(U,Y)O_x$. These capsules were irradiated for 198.87 days in the HFR Petten. The burn-up of the U-bearing capsules was 17–20% FIMA. The present paper describes all aspects of the EFTTRA-T3 irradiation; the fabrication and characterisation of the samples, irradiation and both destructive and non-destructive PIE.

PACS: 61.80.Hg; 81.05.Mh; 61.16.–d

1. Introduction

Radioactive waste from spent fuels represents a radiological risk for a long period of time (>100 000 years). The long-term radiotoxicity of this waste is mainly determined by the actinides plutonium and americium. Transmutation of these actinides offers a possibility for the reduction of the radiotoxicity of nuclear waste. Within the EFTTRA [1] framework innovative concepts for transmutation targets are studied. Presently the research of the EFTTRA group focuses on the development of targets for the transmutation of americium. This is performed in a step-wise approach, by irradiating inert matrices [1,2], inert matrices with uranium oxide ([3,4] and this work) and selected inert matrices with americium [5–7].

In the present irradiation experiment (EFTTRA-T3) uranium simulates the actinides to be transmuted (e.g. Pu or Am). An advantage is that uranium can be handled more easily than plutonium or americium containing material. A disadvantage of uranium is that, with regard to some aspects, its behaviour is different from that of Pu and Am. The main difference is that the helium production of Pu and especially Am containing fuel is larger than that of U-containing fuels. Am-containing fuels show a strong swelling [5,7], which is observed to be much less in the presently studied U-containing fuels. Inert matrices with and without uranium were irradiated, to discriminate the effect of fission products from that of neutrons. It is not the aim to be fully representative for the conditions in any future large-scale industrial transmutation scenarios. Due to the rather general aim of the present experiment, the results are relevant to both LWR and fast reactor applications.

For inert matrix fuels two concepts are generally considered; (a) a solid solution of the inert matrix material and the fissile material (b) a dispersion-type composite of fissile particles in an inert matrix phase. In the EFTTRA-T3 experiment CerCer dispersion-type fuels were tested. Both micro-dispersion (sub-micron) and macro-dispersions (100–300 μm range) of UO_2 in an inert matrix were irradiated, so that the effect of the fissile particle size could be assessed. In two of the fuels

* Corresponding author. Tel.: +31-224 564 362; fax: +31-224 568 608.
E-mail address: schram@nrg-nl.com (R.P.C. Schram).

[1] Experimental Feasibility of Targets for TRAnsmutation, a European collaboration between CEA, NRG, EdF, FZK, JRC-ITU and JRC-IE.

0022-3115/03/$ - see front matter
doi:10.1016/S0022-3115(03)00176-4

$(U,Y)O_x$ inclusions (U:Y ratio 1:6) were used (so-called hybrid concept) to study the impact of diluting the fissile material within the fissile inclusions, while keeping the total uranium density constant. Due to the very high burn-up foreseen in the UO_2-particles adverse effects may occur (e.g. large swelling, high fission-gas release) which may be prevented by decreasing the local concentration of fissile material, as is done in the $(U,Y)O_x$ particles.

In this paper, the results of the fabrication, irradiation and post irradiation test of the EFTTRA-T3 experiment are discussed.

2. Experimental

2.1. Sample preparation

Five inert matrices were selected: CeO_{2-x}, Y_2O_3, MgO, $MgAl_2O_4$ and $Y_3Al_5O_{12}$. The powders of all these matrices were obtained commercially, but powders for MgO and $MgAl_2O_4$ were prepared at NRG using the precipitation technique for some targets (indicated in Table 1). The fuel test matrix is presented in Table 1. The fissile targets contained about 2.5 vol.% UO_2 or 19.6 vol.% $(U,Y)O_x$, both enriched with 20% ^{235}U. In addition, $BaZrO_3$ without a fissile phase was irradiated as a candidate inert matrix.

Pellets containing $CeO_{2-x} + UO_2$, $Y_2O_3 + UO_2$, $MgO + UO_2$, $MgAl_2O_4 + UO_2$ $Y_3Al_5O_{12} + UO_2$ were manufactured by mixing UO_2 particles and the inert matrix powders in an agate mortar. These UO_2 particles were prepared by the sol–gel technique and the particle diameter after sintering was in the order of 100–300 μm. A minor fraction of very small UO_2 particles (<10 μm) was observed on the surface of the UO_2 particles before sintering.

$MgAl_2O_4 + UO_2$ pellets were prepared by co-precipitation. These pellets contained small (<1 μm) UO_2 particles, which allowed to study the effect of the particle size on irradiation behaviour. The co-precipitated $MgAl_2O_4 + UO_2$ has been made by dissolving MgO, $Al(NO_3)_3 \cdot 9H_2O$ and UO_2 in nitric acid, followed by precipitation by NH_4OH addition. The obtained powder has been cleaned with amongst others acetone and calcined at 800 °C.

$(U,Y)O_x$ particles were made by dissolving UO_2 and Y_2O_3 in HNO_3, followed by precipitation by adding NH_4OH. They were subsequently cleaned in amongst others acetone and calcined at 800 °C. The $MgO + (U,Y)O_x$ and $MgAl_2O_4 + (U,Y)O_x$ targets were made by mixing inert matrix powder with the $(U,Y)O_x$ particles. The volume fraction of the $(U,Y)O_x$ phase in these pellets was 19.6 vol.%.

Green pellets of all the powders were prepared by uni-axial pressing. The applied pressure ranges from 255 to 640 MPa. Dies with a diameter of 6.0, 6.5 and 7.0 mm were used. The green uranium containing pellets were sintered under reducing conditions ($Ar/H_2 = 95/5$) for 5 h at a temperature of 1600 °C. The inert matrix pellets were sintered in air for 5 h at temperatures of 1600–1700 °C. The geometrical densities of the targets are shown in Table 1. The average pellet diameter after sintering ranges from 5.08 to 5.49 mm, which yields a gap between pellet and cladding of 80–285 μm (Table 1). The pellets were loaded in 15/15 Ti steel capsules provided by CEA. The capsules had a length of 168 mm and an inner diameter of 5.65 mm. About 70 mm of sample material

Table 1
Description of the EFTTRA-T3 targets

No.	Target	Density (% TD)	Gap (μm)	Stack length (mm)	Number of pellets
1	$CeO_{2-x} + UO_2$	87 ± 2	150 ± 20	69	6
2	CeO_2	93 ± 1	210 ± 10	72	7
18	$Y_2O_3 + UO_2$	95 ± 1	160 ± 10	73	15
4	Y_2O_3	96 ± 1	140 ± 10	81	17
5	$MgO^{(cp)} + UO_2$	89 ± 3	190 ± 20	70	15
6	$MgO^{(cp)}$	90 ± 1	210 ± 20	80	15
7	$MgO + (U,Y)O_x^{(cp)}$	81 ± 5	270 ± 80	76	12
8	MgO	82 ± 3	80 ± 20	82	18
9	$(MgAl_2O_4 + UO_2)^{(cp)}$	90 ± 3	290 ± 40	68	12
10	$MgAl_2O_4^{(cp)}$	96 ± 1	200 ± 20	81	16
11	$MgAl_2O_4 + UO_2$	95 ± 1	220 ± 20	69	12
12	$MgAl_2O_4$	95 ± 1	220 ± 20	81	15
13	$MgAl_2O_4 + (U,Y)O_x^{(cp)}$	92 ± 1	220 ± 10	70	13
14	$BaZrO_3$	74 ± 1	200 ± 50	79	16
15	$Y_3Al_5O_{12} + UO_2$	90 ± 1	130 ± 10	71	12
16	$Y_3Al_5O_{12}$	93 ± 1	170 ± 10	81	17

(cp) These compounds were made by (co)-precipitation.

was loaded in each capsule. The pellets were separated from the steel plugs by inert matrix plugs, which were made of the same material as the inert matrix of the sample material. The capsules were welded under helium atmosphere (1 bar). Prior to irradiation the closed capsules were inspected using X-ray photography [4].

2.2. Sample characterisation

Before irradiation, the macro-dispersed fissile particles could be clearly discerned from the inert matrix phase on all ceramographies. Ceramographies made on the pellets containing the 100–300 μm UO_2 particles showed that during the uni-axial pressing of these pellets, the UO_2 particles were deformed into ellipsoids. The ceramographies showed that the $(U,Y)O_x$ inclusions had a rather irregular shape and a size of 100–200 μm after sintering. Analysis (ICP-AES, IDMS) showed that the U:Y ratio in $(U,Y)O_x$ particles is 1:6.

X-ray diffraction (as well as EPMA and α-autoradiographs after irradiation) showed that no chemical interaction occurred between UO_2 and the inert matrices: MgO, $MgAl_2O_4$ and $Y_3Al_5O_{12}$ after sintering of the pellets. As expected from phase diagrams [7], MgO and Al_2O_3 do not form a solid solution with UO_2 under reducing conditions, which could explain the absence of chemical interaction between UO_2 and both MgO and $MgAl_2O_4$ in the present experiment. No literature data has been found on possible chemical interaction between $Y_3Al_5O_{12}$ and UO_2, but since Y_2O_3 can form a solid solution with UO_2 [8] it can not be excluded that this chemical interaction may occur. However, for the present experiment no interaction between $Y_3Al_5O_{12}$ and UO_2 was observed.

X-ray diffraction on $Y_2O_3 + UO_2$ showed the presence of Y_2O_3, UO_2 and a fluorite phase that is probably a $(U,Y)O_x$ solid solution [8]. In $CeO_{2-x} + UO_2$ a range of fluorite phases could be identified in addition to CeO_{2-x} and to UO_2, which can be attributed to a $(Ce,U)O_{2-x}$ solid solution. The fluorite structure of CeO_{2-x} can only be found for $0 < x < 0.17$ [8], indicating that the present pellets were in this stoichiometry range.

In the $(U,Y)O_x$ containing pellets $(MgO + (U,Y)O_x$ and $MgAl_2O_4 + (U,Y)O_x)$ X-ray diffraction prior to irradiation showed besides MgO and $MgAl_2O_4$, the presence of amongst others several fluorite phases, attributed to the $(U,Y)O_x$ particles.

3. Irradiation conditions

The 16 capsules were loaded in the EFTTRA-T3 sample holder, which was irradiated for 198.87 full power days in the HFR-Petten. The capsules were placed at two different axial levels, causing the neutron flux in the capsules 1, 2, 4, 5, 6, 7, 8 and 18 to be about 20% lower than in the capsules 9, 10, 11, 12, 13, 14, 15 and 16. The temperature of the aluminium support of the capsules was kept at 600 ± 25 K during the irradiation. The temperature of the inert matrices was calculated to be 640–690 K and that of the U-bearing matrices 700–1000 K during the irradiation. These temperatures of the fissile targets are estimated taking into account changes of gas-composition, swelling and decrease of the fission power. Fig. 1 shows the axial positions of the capsules and the thermal and fast neutron fluences as deduced from gamma-scan wire measurements.

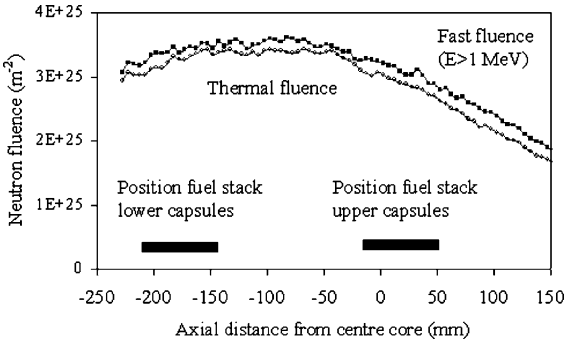

Fig. 1. The deduced neutron fluences and the position of the capsules.

Table 2 shows the neutron fluences, as determined using neutron fluence detector sets, the calculated burn-up and the fission power at begin of irradiation (BOI) and at end of irradiation (EOI). From the data shown in Table 2 it can be concluded that the fluence, power and the burn-up variation between the various capsules is relatively small and therefore it is unlikely that these differences induce a large difference in the behaviour during irradiation between the various capsules.

4. Non-destructive examination

4.1. Profilometry

The eight uranium containing capsules were inspected by profilometry in order to determine any deformation of the cladding. Only the cladding of capsule 15 ($Y_3Al_5O_{12} + UO_2$) showed a diameter increase of about 0.2% along the length of the fuel stack (Fig. 2). The $Y_3Al_5O_{12}$ capsule without UO_2 was thereafter also measured for comparison, but no diameter change was observed.

4.2. Gamma scanning

Axial gamma scanning was performed after irradiation on all fissile material containing capsules in order to:

Table 2
Neutron fluence, burn-up and power of the fuel containing capsules

Capsule	1	5	7	9	11	13	15	18
Fluence (10^{25} m^{-2}) 1.353 MeV < E < 19.64 MeV	2.28	2.41	2.32	2.65	2.79	2.81	2.69	2.39
Fluence (10^{25} m^{-2}) 67.34 keV < E < 1.353 MeV	3.91	4.13	3.96	4.52	4.76	4.8	4.59	4.09
Fluence (10^{25} m^{-2}) 0.625 eV < E < 67.34 keV	4.64	4.64	4.75	5.07	5.27	5.39	5.19	4.47
Fluence (10^{25} m^{-2}) 0.0001 eV < E < 0.625 eV	2.67	2.75	2.69	3.27	3.29	3.25	3.26	2.73
Fluence (10^{25} m^{-2}) total	13.5	13.93	13.72	15.51	16.11	16.25	15.73	13.68
Fluence (10^{25} m^{-2}) E > 0.1 MeV	5.89	6.23	5.98	6.82	7.18	7.24	6.93	6.17
Burn-up (% FIMA)	17.1	17.5	17.3	19.1	19.7	19.8	19.3	17.2
Power at BOI (W/cm)	47	45	45	51	56	63	59	50
Power at EOI (W/cm)	17	16	16	18	20	23	21	18

The uncertainty in the fluence is about 2%, the uncertainty in the power and burn-up is 10–15%.

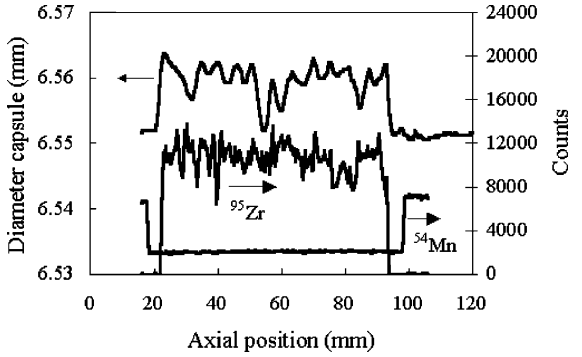

Fig. 2. Profilometry and gamma scan (^{95}Zr, ^{54}Mn) results of capsule 15 ($Y_3Al_5O_{12} + UO_2$). The bottom of the capsule is located at axial position 0 mm.

- Study the length change of the fuel stacks, using an immobile fission product, such as ^{95}Zr. The fuel stack length before irradiation was determined from the sum of the height of the pellets. Fig. 2 shows the results of gamma scans of capsule 15 after irradiation. Note that ^{95}Zr is an immobile fission product and ^{54}Mn is an activation product present in the stainless steel cladding and the steel plugs present in the capsules. The results of these gamma scan measurements were compared with those of the micrometer height measurements (Section 4.3) and reasonable agreement was observed. Since the accuracy of the micrometer measurements is considered to be higher than that of the gamma scans, mainly the results of the micrometer measurements are presented.
- Study the redistribution of potentially mobile fission products (e.g. ^{134}Cs or ^{137}Cs). In the capsules 1 ($CeO_{2-x} + UO_2$), 7 ($MgO + (U,Y)O_x$), 11 ($MgAl_2O_4 + UO_2$, macro-dispersed) and 15 ($Y_3Al_5O_{12} + UO_2$) a minor caesium migration out of the fissile stack was observed. For the other isotopes no redistribution could be observed, except for a small amount of pellet fragments that broke off from the pellet stack.

4.3. Dimensional measurements

Dimensional measurements were performed on the pellets before and after irradiation using a micrometer. All $BaZrO_3$ pellets were broken after irradiation, suggesting that this material is not a suitable inert matrix. It is however unclear if these pellet fractures can be partially be attributed to the relatively low density of the $BaZrO_3$ pellets before irradiation (74% TD).

Table 3 shows the dimensional changes of the pellets measured with a micrometer and in a few cases gamma scanning, ceramography and profilometry. The changes in height and diameter are used to calculate the change in volume. Mass measurements on the pellets without UO_2 show that in a few cases the pellets lost some mass, due to breaking of fragments from the pellets. The large negative volume change measured for capsule 12 ($MgAl_2O_4$), can be attributed to mass loss and is therefore not intrinsic to $MgAl_2O_4$. The significant volume decrease observed for $CeO_{2-x} + UO_2$ is not due to any mass loss, but is an intrinsic effect. The large volume swelling of $MgAl_2O_4 + UO_2$ is caused by axial swelling due to the formation of radial cracks. The other pellets containing a fissile phase (except $Y_3Al_5O_{12} + UO_2$) and all inert matrices without fissile phase show only minor volume changes under these EFTTRA-T3 irradiation conditions. The currently observed very small dimensional changes in the matrices $MgAl_2O_4$ (capsule 10), CeO_2 and $Y_3Al_5O_{12}$ are in good agreement with the results obtained on these matrices in the EFTTRA-T2 and EFTTRA-T2-bis irradiations [1,2], which were done under similar conditions to a similar neutron fluence.

Table 3
Dimensional changes and fission-gas release after irradiation

Matrix	Inert matrix		Inert matrix + fissile phase					
	No.	$\Delta V/V$ (%)	Fissile phase	No.	$\Delta h/h$ (%)	$\Delta d/d$ (%)	$\Delta V/V$ (%)	FGR (%)[a]
CeO_2	2	0.6 ± 0.1	UO_2	1	-2.5 ± 0.8[b]	-1.2 ± 0.7	-4.9 ± 1.5	8
Y_2O_3	4	-0.4 ± 0.3	UO_2	18	-1.3 ± 0.4	-0.1 ± 0.1	-1.4 ± 0.4	5
MgO	6	-1.7 ± 1.0[c]	UO_2	5	0.1 ± 0.6	0.4 ± 0.4	0.9 ± 1.0	4
MgO	8	0.5 ± 0.2	$(U,Y)O_x$	7	-0.4 ± 0.4	0.1 ± 0.5	-0.3 ± 1.1	3
$MgAl_2O_4$	10	-0.6 ± 0.3	UO_2	9	-1.0 ± 0.3	0.1 ± 0.5	-0.8 ± 1.0	0.1
$MgAl_2O_4$	12	-3.6 ± 0.2[c]	UO_2	11	5.1 ± 0.6	0.7 ± 2.5[d]	6.5 ± 5.0	43
$MgAl_2O_4$			$(U,Y)O_x$	13	0.6 ± 0.3	1.2 ± 0.2	2.9 ± 0.6	3
$BaZrO_3$	14	–[e]						
$Y_3Al_5O_{12}$	16	-1.1 ± 0.3	UO_2	15	0.5 ± 0.8[b]	5.0 ± 0.4[f]	10.5 ± 1.1	47

[a] The relative error in fission-gas release (FGR) is about 10%.
[b] Gamma scan.
[c] Mass loss (see text).
[d] Ceramography.
[e] Not measured pellets broken.
[f] Profilometry.

4.4. Fission-gas release

Gas puncturing of the fissile material containing capsules revealed that all capsules remained intact during irradiation. The composition of the gases has been analysed using mass spectrometry. The results of the neutronics computations were combined with the gas puncturing results in order to obtain the fission-gas release (Table 3). The release fractions of Kr and Xe were similar, as expected.

5. Ceramography, EPMA and α- and β/γ-autoradiography

The microstructure of the samples and the distribution of the fission products in these samples has been studied using ceramography, electron probe micro analysis (EPMA) and α-, β/γ-autoradiography. All eight fissile material containing samples have been studied with one or more EPMA line scans and X-ray maps. The results of the line scans have been corrected for absorption differences using the ZAF technique, while the X-ray maps could not be corrected. The following sections show typical examples of ceramography, EPMA and α-, β/γ-autoradiography results.

5.1. $MgAl_2O_4$ containing micro-dispersed UO_2

The result of a radial scan in the $MgAl_2O_4$ containing micro-dispersed UO_2 is shown in Fig. 3. A relatively constant distribution of the three elements measured from the pellet edge to the pellet centre can be observed. The centre of the pellet experienced a higher temperature than the edge of the pellet and therefore different behaviour might have occurred (e.g. a lower Xe-retention), which is however not observed. The EPMA probed volume (which is a few cubic micron) is larger than the typical volume of a UO_2 particle (which is a 0.1 μm^3 or less). Given this ratio of these volumes and the volume fraction of UO_2 in the present sample it can be estimated that in the EPMA probed volume 3–10 UO_2 particles are present, which explains the scatter in the U-measurement data in Fig. 3. The scatter in the Xe and the Zr measurement data is small since the recoil range of the fission products is about 10 μm, which causes a rather homogeneous distribution of these fission products.

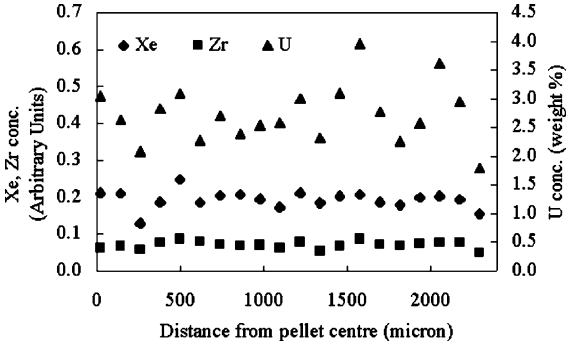

Fig. 3. The concentration profiles of U, Zr and Xe in $MgAl_2O_4$ containing micro-dispersed UO_2. The data for Xe and Zr are shown in arbitrary units, since the low magnitude of the signal makes the accuracy of the absolute values relatively low.

5.2. CeO_{2-x} containing macro-dispersed UO_2

The microstructure of the irradiated $CeO_{2-x} + UO_2$ sample is shown in Fig. 4. The porous centre is a UO_2

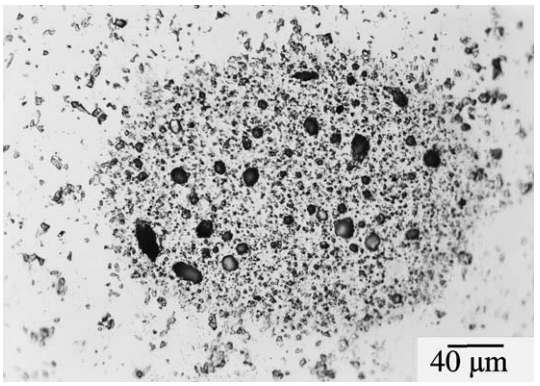

Fig. 4. Ceramography of the $CeO_{2-x} + UO_2$ sample (after irradiation).

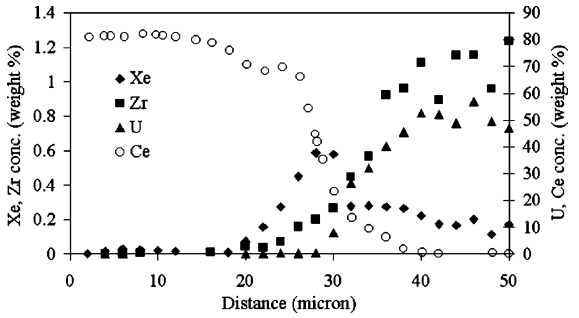

Fig. 5. The concentration profiles of Ce, U, Xe and Zr in the UO_2/CeO_{2-x} sample.

particle. Ceramography shows that the irradiated UO_2 particles in all five inert matrices have a highly porous structure. An EPMA line scan from the CeO_{2-x} matrix into a UO_2 particle was recorded (Fig. 5). The following remarks can be made:

- The Ce signal in the CeO_{2-x} phase is rather smooth, while it shows a large scattering in the UO_2 phase. This scatter is due to the high porosity in the UO_2 phase.
- The relatively broad interface between the CeO_{2-x} phase and the UO_2 phase (10–15 μm) is due to the local formation of a $(Ce,U)O_{2-x}$ solid solution. A similar narrow region around the UO_2 particles in which a solid solution is formed is observed in $UO_2 + Y_2O_3$. In the matrices MgO, $Y_3Al_5O_{12}$ and $MgAl_2O_4$ such solid-solution regions are not observed with UO_2.
- The presence of Xe and Zr in the CeO_{2-x} at positions where no U is present corresponds to the typical recoil range of fission product atoms into a ceramic matrix of about 10 μm (Fig. 5). Further away from the recoil range no fission products can be detected, which shows that transport of fission products into the inert matrix induced by for instance thermal diffusion is small or absent.
- A peak in the Xe-concentration exists at the interface between the UO_2 particle and the CeO_{2-x} region. This peak in the Xe-concentration is also observed in the interface region of all the other UO_2 containing matrices presently studied (e.g. Fig. 6). The spatial distribution of Xe due to recoil is similar to that of Zr, but not all Xe implanted in the UO_2 matrix is measured, which is a combination of two effects:
  1. Fission-gas release from the UO_2 particles.
  2. A large fraction of the xenon is contained in the pores present in the UO_2 phase. This fraction can not be measured using EPMA since cutting of the pellets causes release of the xenon. Therefore the actual Xe-concentration in the UO_2 particle can be much higher than derived from the EPMA results.

These two effects decrease the measured Xe-concentration in the UO_2. Since in the CeO_{2-x} phase close to the interface no high porosity is present, a higher Xe-concentration is measured at this location, which results in the observation of a peak in the Xe-concentration. The other fission products that have been studied using EPMA are Cs and Nd. Nd does not show migration in all of the matrices measured, while Cs shows a minor redistribution in some cases. The EPMA results on the high burn-up porous Pu-rich islands in inhomogeneous MOX fuel [9] show similar behaviour, being almost complete retention of Cs and Nd. In these Pu-islands most of the xenon was released into pores causing the maximum Xe-concentration measured using EPMA to be about 0.3 wt%, which is similar to the presently measured Xe-concentrations in the UO_2 phase (between 30 and 50 μm in Fig. 5).

5.3. MgO containing macro-dispersed UO_2

X-ray maps on the $MgO + UO_2$ sample are shown in Fig. 6. The U-distribution shows the location of the UO_2 particle. The rest of the figure shows the MgO matrix. The Xe-distribution shows a clear increase in the concentration at the interface between the MgO matrix and the UO_2 particle. The line scans show that in the centre of the MgO phase no Xe is present. Some background signal is found on the Xe and Zr mapping. The Xe signal in the centre of the UO_2 particles (which is somewhat higher than that in centre of the MgO matrix), is the sum of the background signal and the Xe remaining in the UO_2 matrix. The observed behaviour of Xe is in agreement with the line scans that show that a small amount of Xe remains in the UO_2 particles (e.g. Fig. 5). The Zr-distribution is similar to that of the U-distribution, but for Zr the 10-μm recoil range into MgO is observed.

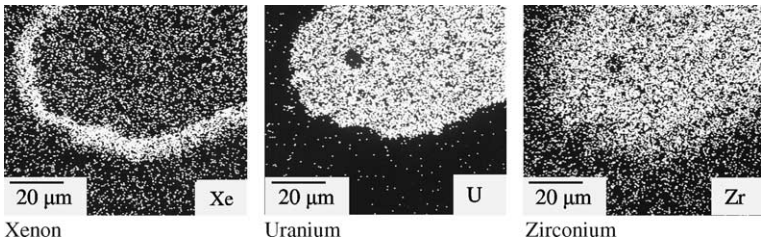

Fig. 6. X-ray maps of Xe, U and Zr in the $MgO + UO_2$ sample.

5.4. MgO containing macro-dispersed $(U,Y)O_x$

The X-ray maps of Xe, U and Nd are shown in Fig. 7. The figures are less pronounced than those in Fig. 6, which is amongst others due to the lower concentration of U-atoms in the fissile phase and the somewhat smaller magnification. Outside of the U-containing region MgO is present. The maps results of U,Y and Mg (the latter two are not shown) show that the $(U,Y)O_x$ phase and the MgO phase do not chemically interact, which is in agreement with ceramography results. The U:Y-ratio is approximately constant in the $(U,Y)O_x$ phase. The maps of Xe and of the immobile fission products Nd are similar, showing that Xe is retained in the fissile phase, which is strongly different from the behaviour of Xe observed in the UO_2 particles (Fig. 6). The fission product maps show a similar penetration depth of about 10 μm in the inert matrix as observed in the other capsules. Ceramographies show that the porosity in the $(U,Y)O_x$ phase is low.

5.5. $MgAl_2O_4$ containing macro-dispersed $(U,Y)O_x$

For $MgAl_2O_4 + (U,Y)O_x$ it is shown by EPMA results and ceramographies (Fig. 8) that the chemical interaction between the fissile phase and the matrix is much stronger than in the case of $MgO + (U,Y)O_x$. Three grades of grey are observed in Fig. 8, of which the compositions have been identified using EPMA. The darkest grey (outer region) is the $MgAl_2O_4$ matrix. The

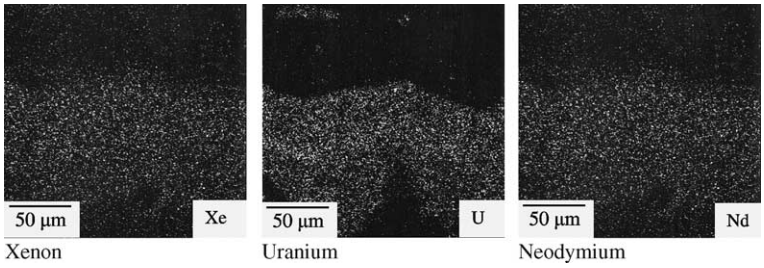

Fig. 7. X-ray maps of U, Xe and Nd in the $MgO + (U,Y)O_x$ sample.

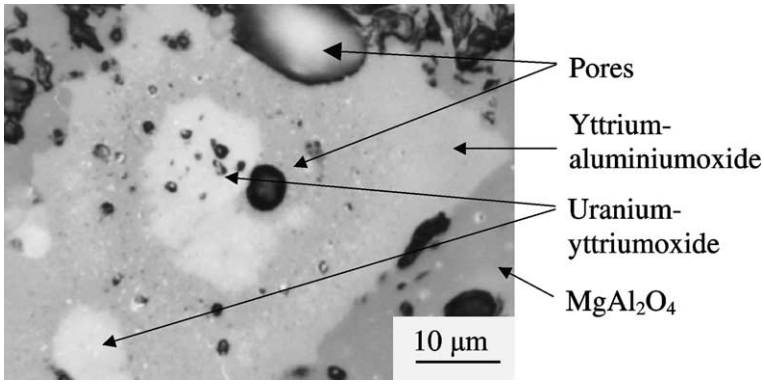

Fig. 8. Ceramography of $MgAl_2O_4$ containing $(U,Y)O_x$ (after irradiation).

medium grey region contains an yttrium–aluminiumoxide in which no Mg and U are present. The lightest grey region contains a uranium–yttriumoxide in which no Mg and Al are present. These results show that $MgAl_2O_4$ has significant chemical interaction with the $(U,Y)O_x$ phase.

Due to the formation of the yttrium–aluminiumoxide phase, the fraction of Y-atoms which is present in the uranium–yttriumoxide phase decreased, which increased the U-concentration in the uranium–yttriumoxide phase. The high U-concentration increased the density of fission products in the uranium–yttriumoxide phase. The Xe-maps in the uranium–yttriumoxide phase show a partial release of Xe from the uranium–yttriumoxide phase. Fig. 8 shows that the porosity in the uranium–yttriumoxide phase is much smaller than that in the irradiated UO_2 particles.

5.6. $Y_3Al_5O_{12}$ containing macro-dispersed UO_2

Fig. 9 shows a ceramograph of irradiated $Y_3Al_5O_{12}$ containing macro-dispersed UO_2. The highly porous structure of the UO_2 particle is similar to that in the macro-dispersed UO_2 particles in the other matrices (e.g. Fig. 4, $CeO_{2-x} + UO_2$). For this UO_2 particle it can be observed that there exists a combination of fine porosity (<10 μm) and one large pore, which has similar dimensions as the UO_2 particle. For UO_2 particles in some of the other matrices this phenomenon can also be observed. For $Y_3Al_5O_{12}$ it is observed that the 10 μm recoil region surrounding the UO_2 particle has become highly porous, similar to the UO_2 phase.

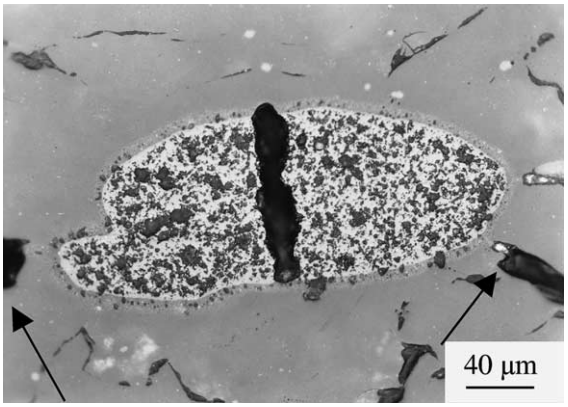

Fig. 9. Ceramography of $Y_3Al_5O_{12}$ containing macro-dispersed UO_2 (after irradiation). The arrows mark the start of cracks that penetrate through the complete matrix.

5.7. α- and β/γ-autoradiography

The α-autoradiographs of four irradiated pellets are shown in Fig. 10 as typical examples. Micro-dispersed $MgAl_2O_4 + UO_2$ (capsule 9) shows a homogenous uranium distribution (except for some small regions where black dots suggest a lower uranium concentration). The few white dots shown in the α-autoradiograph of capsule 9 are an artefact due to damage of the film. The α-autoradiographs of $MgAl_2O_4 + UO_2$, $Y_3Al_5O_{12} + UO_2$ and $MgO + UO_2$ show areas with distinct white spots (the fissile regions) and a black surrounding (the inert matrix). The α-autoradiographs of $Y_2O_3 + UO_2$ and of $CeO_{2-x} + UO_2$ shows the presence of grey areas (besides white and black areas), which points to regions containing a low concentration of uranium. The α-autoradiographs of $MgAl_2O_4 + (U,Y)O_x$ and of $MgO + (U,Y)O_x$ show much larger white areas, which can be attributed to the high concentration of fissile phase. The β/γ-autoradiographs of all the uranium containing materials show that the distribution of the fission products is similar to that of the uranium as deduced from the α-autoradiographs. This shows that no large-scale redistribution of fission products (e.g. caesium) occurred.

6. Discussion

In the EFTTRA-T3 experiment a large variety of targets has been irradiated. The aim of the present discussion is to compare the results of:

- the use of micro versus macro dispersed fissile particles;

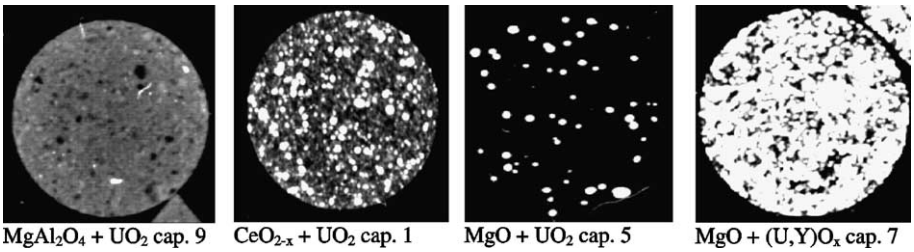

Fig. 10. The α-autoradiographs of four capsules.

Table 4
Qualitative comparison of the results of the fissile material containing targets

Target	Dimensional stability	Pellet integrity	Fission-gas retention	Chemical stability
$CeO_2 + UO_2$	±	+	±	±
$Y_2O_3 + UO_2$	+	+	±	±
$MgO + UO_2$	+	±	±	+
$MgO + (U,Y)O_x$	+	+	±	+
$MgAl_2O_4 + UO_2$ (micro-dispersed)	+	+	++	[a]
$MgAl_2O_4 + UO_2$	−	−	–	+
$MgAl_2O_4 + (U,Y)O_x$	±	+	±	−
$Y_3Al_5O_{12} + UO_2$	–	−	–	+

[a] The chemical form of the uranium after the irradiation could not be determined.

- the dilution of the fissile phase $(U,Y)O_x$ versus the use of UO_2;
- the various matrices.

In order to facilitate the comparison, the main results of the uranium containing pellets are summarised in Table 4. The materials are compared in the categories: dimensional stability, pellet integrity, fission-gas retention and chemical stability. Materials with a good dimensional stability have a small volume change during irradiation. A volume increase during irradiation is considered more adverse than a volume decrease. The pellet integrity is judged from the density of cracks in the pellets. The chemical stability is judged from the chemical interaction between the matrix phase and the fissile phase.

6.1. The use of micro- versus macro-dispersed fissile particles

In the present study only one micro-dispersed fuel was irradiated ($MgAl_2O_4 + UO_2$), while seven macro-dispersed fuels were irradiated. The observed behaviour of this one micro-dispersed fuel was very good, since it has a good dimensional stability, the lowest fission-gas release of all samples and good pellet integrity after the irradiation. However, in the EFTTRA-T4ter irradiation [7] and the Thermet irradiation [10], which both contained co-precipitated UO_2 and $MgAl_2O_4$, but with a higher volume fraction of UO_2, it has been observed that this compound shows large volume swelling. These two experiments strongly suggest that micro-dispersed $MgAl_2O_4$-based targets are not suitable for transmutation purposes. In addition the EFTTRA-T4 [5] and the EFTTRA-T4bis [7] experiments on targets of micro-dispersed americium in $MgAl_2O_4$ also show large swelling. The presently observed good behaviour of the micro-dispersed UO_2 in $MgAl_2O_4$ is probably due to the relatively low concentration of fissile atoms. For $MgAl_2O_4$, it appears that macro-dispersed is preferable. For the other candidate inert matrices it is not yet clear if macro-dispersed or micro-dispersed fuel is to be preferred from the viewpoint of irradiation stability.

6.2. The dilution of the fissile phase $(U,Y)O_x$ versus the use of UO_2

Two of the macro-dispersed fuels contained $(U,Y)O_x$ inclusions, while five of the macro-dispersed fuels contained UO_2 inclusions. The total uranium quantity in all pellets was approximately constant. In these UO_2 particles a very high porosity was observed (e.g. Fig. 4), which is due to the high uranium burn-up. Such a high burn-up is also known to create porous regions in standard UO_2 pellets (rim effect). The structure of the irradiated UO_2 particles can also be compared with that in plutonium-rich islands in irradiated inhomogeneous MOX fuel [9], having a similar high local burn-up (about 20% FIMA). In these plutonium rich particles a similar very small grain size and increase of porosity is observed after irradiation. In CeO_{2-x} and Y_2O_3 the porosity in the UO_2 phase is about 30%, as determined by image analysis. In $MgAl_2O_4$ and $Y_3Al_5O_{12}$ the porosity in the UO_2 phase is about 40%. The porosity in the UO_2 phase in MgO could not be measured accurately, but is estimated to be 30–40%. The porosity and the formation of solid fission products causes a swelling of the UO_2 particles in the range of 50–80 vol.% [11].

For the $(U,Y)O_x$ phase in both $MgAl_2O_4$ and MgO it is observed that during irradiation the porosity decreased with about 5–10%. For the $(U,Y)O_x$ phase in MgO it can be observed that before irradiation the porosity of this phase is about 10%, while after irradiation the porosity is nearly absent. In $(U,Y)O_x + MgAl_2O_4$ it is observed in the fissile phase that the initial porosity of 20% decreased to about 10% after irradiation. Due to the observed decrease in porosity and the low concentration of fission products in the $(U,Y)O_x$ particles it is likely that the $(U,Y)O_x$ particles show much smaller swelling (if any) than the UO_2 particles. This assumption of the smaller swelling of $(U,Y)O_x$ particles compared to UO_2 particles is supported furthermore by two phenomena:

- A somewhat smaller swelling of the $(U,Y)O_x$ containing matrices compared to the UO_2 containing matrices (Table 3).
- Smaller crack widths in the matrices containing $(U,Y)O_x$ particles, compared to those containing UO_2 particles.

The Xe distribution in the UO_2 phase, in the uranium–yttriumoxidephase in $MgAl_2O_4 + (U,Y)O_x$ and in $MgO + (U,Y)O_x$ suggests that above a certain Xe-concentration threshold Xe-atoms are released from the matrix of the uranium containing phase into pores in the uranium containing phase. In the samples where with EPMA a good Xe-retention in the solid material of the fissile phase is observed, the porosity formation in the fissile phase is low. For the present EFTTRA-T3 conditions it can be concluded that the hybrid concept tends to decrease the porosity formation and the fission-gas release (Table 3) and improves the xenon retention in the matrix of the fissile phase and the dimensional stability of the fuel pellets.

6.3. Comparison of the various matrices

In order to compare the inert matrices that were studied in the present research ($Y_3Al_5O_{12}$, $MgAl_2O_4$, CeO_{2-x}, Y_2O_3 and MgO), their behaviour containing macro-dispersed UO_2 is evaluated.

Before and after irradiation Vickers hardness and fracture toughness measurements have been performed on the matrices [11]. It is concluded that no extremely large variation exists in the properties of these matrices and that the impact of irradiation on the mechanical properties is less than 70%. Evaluation of the mechanical behaviour of composites [11] shows that the large swelling of the fissile inclusion (50–80 vol.%) causes mechanical stress, which is expected to induce fracture of the matrix (e.g. Fig. 9). Under the present irradiation conditions cracks between the UO_2 particles were expected in all matrices, but are only observed in the matrices $Y_3Al_5O_{12}$, $MgAl_2O_4$ and MgO. The matrices CeO_{2-x} and Y_2O_3 did almost not show fracture between the UO_2 particles, which might be attributed to creep of these matrices. The smaller tendency for the CeO_{2-x} and Y_2O_3 pellets to break is an advantage of these compounds.

The EPMA data (e.g. Figs. 5 and 6) show that the inert matrices studied (except $Y_3Al_5O_{12} + UO_2$) can retain high concentrations of fission products under the temperature conditions of the EFTTRA-T3 irradiation. The bubble formation in the $Y_3Al_5O_{12}$ interface region in $Y_3Al_5O_{12} + UO_2$ (Fig. 9) shows that the fission-gas concentration came above the solubility limit for $Y_3Al_5O_{12}$, which suggests that the gas retention properties of $Y_3Al_5O_{12}$ are not as good as those of the other matrices. For fissile particles that are much larger than the fission-product recoil range it can be shown mathematically that the concentration of fission products implanted directly at the fuel/matrix interface is half of the concentration in the centre of the particles [12]. Making a detailed experimental analysis of the fission-product concentration in the interface region is complex, but the present results (e.g. Fig. 5) suggest that most of the fission products implanted in the matrices remain on the position where they are implanted and that no thermal diffusion or release occurred.

No solid solution formation is observed between the UO_2 phase and the inert matrices MgO, $MgAl_2O_4$ and $Y_3Al_5O_{12}$, while in the case of Y_2O_3 and CeO_{2-x} a solid solution has probably formed with the UO_2 particles with a typical width of 10–20 μm.

The EFTTRA-T3 irradiation yields the following conclusions on the suitability of the various matrices:

- $Y_3Al_5O_{12}$ seems to be the least suitable matrix, since a large diametrical swelling, pellet fracturing and a high fission-gas release are observed. The high fission-gas release is presumably caused by fracturing of the pellets, which provides release paths to the plenum. It should be remarked that the UO_2 particles have a very high burn-up, are highly porous, such that high gas release from the particles may be expected. The concentration of fission-gas atoms that can be implanted in the $Y_3Al_5O_{12}$ phase without pore formation is lower than in the other matrices. This has been derived from comparison of Fig. 9 ($Y_3Al_5O_{12} + UO_2$), with ceramographs of the other matrices.
- $MgAl_2O_4$ is probably also not a very suitable matrix, considering the high fission-gas release, pellet fracturing and axial swelling. In $MgAl_2O_4 + (U,Y)O_x$ a chemical interaction layer between the matrix and the fissile phase is observed. Fuel fabrication experiments using $MgAl_2O_4 + (Y,Pu,U,Zr)O_{2-x}$ also showed chemical interaction between the matrix and the fissile phase at high temperature [13]. The tendency of $MgAl_2O_4$ to chemically interact with the hybrid phase is a disadvantage of $MgAl_2O_4$. Such a chemical interaction complicates the modelling of the fuel and can amongst others form a chemical compound which has a low melting temperature.
- The behaviour of the matrices CeO_{2-x}, Y_2O_3 and MgO in the present study is quite good. Their behaviour is similar, except for MgO that shows cracks between the UO_2 inclusions, while such crack are (almost) absent in CeO_{2-x} and Y_2O_3.

7. Conclusion

For the EFTTRA-T3 irradiation 16 capsules were successfully irradiated. During the irradiation all capsules remained intact. For all matrices in which no fissile

phase is present, it is observed that the pellets show good dimensional stability and are resistant to neutron irradiation, except for $BaZrO_3$.

$MgAl_2O_4$ with micro-dispersions of UO_2 shows good dimensional stability and a very low fission-gas release, although other experiments [7,10] show that this micro-dispersed compound exhibits strong swelling for higher uranium densities. $Y_3Al_5O_{12}$ and $MgAl_2O_4$ with macro-dispersions of UO_2 show extensive crack formation and a fission-gas release of more than 40%. The extensive diametrical swelling of $Y_3Al_5O_{12} + UO_2$ suggests that $Y_3Al_5O_{12}$ is not suitable to be used as an inert matrix. The UO_2 containing matrices CeO_{2-x} and Y_2O_3 show very few cracks in the pellets after irradiation. The UO_2 containing matrices CeO_{2-x}, MgO and Y_2O_3 show a swelling of less than 1 vol.% and a fission-gas release of less than 10%. As far as the irradiation behaviour is concerned, these three matrices might be suitable for transmutation purposes, although further investigations are required to confirm this. It should be stressed that the present T3 experiment focussed on neutron and fission product effects, but that for americium transmutation purposes the effects of alpha-damage should be carefully studied.

Comparison of the behaviour of $MgAl_2O_4$ and MgO containing either UO_2 or $(U,Y)O_x$ suggest that the hybrid concept has a positive influence on important fuel properties, such as fission-gas release and dimensional stability.

Acknowledgements

The authors would like to thank H. Hein and J.G. Boshoven for target fabrication, M.R. Roos for some of the image analysis, P. van Vlaanderen for X-ray analysis, J.R.W. Woittiez, B. Beemsterboer and O. Zwaagstra for INAA analysis, A. Paardekooper for neutron dosimetry and C. Sciolla for nuclear computations.

References

[1] R.J.M. Konings, K. Bakker, J.G. Boshoven, R. Conrad, H. Hein, J. Nucl. Mater. 254 (1998) 135.
[2] E.A.C. Neeft, R.J.M. Konings, K. Bakker, J.G. Boshoven, H. Hein, R.P.C. Schram, A. van Veen, R. Conrad, J. Nucl. Mater. 274 (1999) 78.
[3] E.A.C. Neeft, K. Bakker, H.A. Buurveld, J. Minkema, A. Paardekooper, R.P.C. Schram, C. Sciolla, O. Zwaagstra, B. Beemsterboer, J.R.W. Woittiez, P. van Vlaanderen, W.J. Tams, H. Hein, R. Conrad, A. van Veen, Prog. Nucl. Energy 38 (2001) 427.
[4] R.P.C. Schram, K. Bakker, J.G. Boshoven, G. Dassel, H. Hein, R.R. Van der Laan, E.A.C. Neeft, R.J.M. Konings, R. Conrad, Proceedings of Global 99, Wyoming USA, 1999.
[5] R.J.M. Konings, R. Conrad, G. Dassel, B.J. Pijlgroms, J. Somers, E. Toscano, J. Nucl. Mater. 282 (2000) 159.
[6] D. Warin, R.J.M. Konings, P. Martin, J.-M. Bonnerot, G. Vambenepe, R.P.C. Schram, J.C. Kuijper, K. Bakker, R. Conrad, Proceedings of the OECD-NEA P&T IEM Workshop, Korea, October 2002, submitted for publication.
[7] F.C. Klaassen, K. Bakker, R.P.C. Schram, R. Conrad, J. Somers, R.J.M. Konings, Proceedings IMF8, 2002, J. Nucl. Mater., in press.
[8] Phase Equilibria Diagrams Database, American Ceramic Society, NIST, Standard Reference 31, CD-rom, 1994.
[9] C.T. Walker, W. Goll, T. Matsumura, J. Nucl. Mater. 228 (1996) 8.
[10] V. Georgenthum, J. Brillaud, N. Chauvin, M. Pelletier, D. Planck, Prog. Nucl. Energy 38 (2001) 317.
[11] E.A.C. Neeft, K. Bakker, R.L. Belvroy, W.J. Tams, R.P.C. Schram, R. Conrad, A. van Veen, J. Nucl. Mater. 317 (2003) 217.
[12] D.W. White, A.P. Beard, A.H. Willis, UASEC Report TID7546, 1957, also identified as KAPL-P-1849.
[13] R.P.C. Schram, K. Bakker, H. Hein, J.G. Boshoven, R.R. van der Laan, C.M. Sciolla, T. Yamashita, Ch. Hellwig, F. Ingold, R. Conrad, S. Casalta, Prog. Nucl. Energy 38 (2001) 259.